FATIGUE BEHAVIOR IN WOOD UNDER PULSATING COMPRESSION-TORSION-COMBINED-LOADING

Yasutoshi Sasaki

Associate Professor
Graduate School of Bioagricultural Sciences
Nagoya University
464-8601 Nagoya, Japan

Mariko Yamasaki

Graduate Student
Graduate School of Engineering
Nagoya Institute of Technology
466-8555 Nagoya, Japan

and

Fumie Akita

Graduate Student
Graduate School of Bioagricultural Sciences
Nagoya University
464-8601 Nagoya, Japan

(Received September 2005)

ABSTRACT

We have experimentally investigated the effects of cyclic compression-torsion-combined loading on the fatigue behavior and stress-strain properties of wood. Pulsating compression and torsion loadings were applied along and around the longitudinal axis of the rectangular bar specimen (Japanese cypress). According to the relationships between stress and strain during fatigue tests, the secant modulus of the stress-strain curve changed with an increase in the number of loading cycles, and the differences between the curves for compression and shear were observed. We found that the experimental results of fatigue tests were influenced by the combined-stress ratios. Compressive stiffness tended to maintain its initial values during almost all loading cycles to failure. Shear stiffness decreased with increasing number of loading cycles, and the final decrease of shear stiffness was larger as compressive stress became dominant. The failure mode was affected by the combined stress states; typical torsion failure was observed in combined stress states with dominant application of shear stress. In contrast, typical compression failure was observed in combined stress states with dominant application of compressive stress. The failure mode under compressive-shear combined stress states was not affected by the stress level, although, as previously demonstrated, it was affected by the stress level under tensile-shear states.

Keywords: Combined stress, compression, fatigue, shear stiffness, torsion.

INTRODUCTION

In a previous study, we reported the fatigue strength of wood under pulsating tension-torsion combined loading (Sasaki and Yamasaki 2002, 2004; Sasaki et al. 2005). It was demonstrated that fatigue strength could be approximated using Hill's criterion for static strength and that fatigue behavior was influenced by the combined-stress ratios and applied stress levels. Bordering on the combined-stress state in which the tensile and shear stress components were almost equally applied, a trend toward lower stiffness retention differed between tension and shear, and the tensile or torsion failure mode became dominant with dominant stress in combined

stress states. This stress state was recognized as a boundary state for both stiffness retention and failure mode. The stiffness retention in this stress state showed a tendency similar to the stiffness retention in a stress state in which torsion was dominant regardless of the stress level. However, it is well known that wood is stronger in tension than in compression; thus its fatigue properties are likely to depend on the mode of loading.

In this study, we have used the same type of specimen as in the previous study (Sasaki and Yamasaki 2002, 2004), and performed fatigue testing under combined compression and torsion, to investigate the fatigue behavior of wood under multiaxial stresses. In particular, this study focused on the influence of the compression-shear combined-stress ratio on the stress-strain properties and fatigue failure of wood.

MATERIAL AND METHODS

Specimens

Small clear specimens of Japanese cypress (*Chamaecyparis obtusa* Endl.) were processed from air-dried lumber samples. The shape and dimensions of the specimens were the same as in previous studies (Sasaki and Yamasaki 2002, 2004). The specimens were cut to have a rectangular cross-section with their major axis lying in the fiber direction; the dimensions of each specimen were 300 mm × 17.5 mm × 17.5 mm (L × T × R). In the central part of each specimen, a taper was attached to four planes, and a portion with cross-sectional dimensions of 11.5 mm × 11.5 mm and a length of more than 25 mm was prepared. The specimens were cured in the laboratory at 25°C at a relative humidity of 40%, until the specimens reached constant weight. The total number of specimens used in the tests was 100 (Table 1).

Static tests

To determine static strength, uniaxial loading, pure torsion, compression-torsion, and tension-torsion, combined loading tests were carried out. Using these tests, the failure surface was determined; this was used as the standard for fatigue tests. An electrohydraulic servomachine, which could apply axial and torsional loads simultaneously, was used. An axial force was applied in the fiber direction (along L), and torque was applied around the axis in the same direction as L. The procedures for the static loading tests for determining static strength in tension, compression, and shear were as follows: uniaxial loading and pure torsion tests were carried out under a controlled condition using a constant rate of displacement. Axial force was applied at a constant axial displacement rate of 0.01 mm/s and the torque at a constant rotational rate of 0.05 degree/s.

The combined loading tests for determining the failure surface were conducted by the proportional deformation loading method, in which the axial force and torque were applied simultaneously to the test specimen with their displace-

TABLE 1. *Number of specimens used.*

Type of tests	Group (stress state)	Number of specimens	Remarks
Static tests	Pure tension	5	Results of the static tests are reported in previous study (Sasaki and Yamasaki 2002).
	Combined tension-torsion	14	
	Pure torsion	5	
	Combined compression-torsion	12	
	Pure compression	5	
Fatigue tests	Pure torsion: S	18	Two to five specimens were used for each stress level.
	Combined compression-torsion: CA	12	
	Combined compression-torsion: CB	14	
	Combined compression-torsion: CC	8	
	Pure compression: C	7	

ment rates kept constant. By changing the application rates of axial displacement and rotation, a failure surface resulting from the combination of axial stress and shear stress at the time of failure was created, as described below. Each stress was calculated as follows: axial stress was obtained by dividing the axial force by the cross-sectional area of the specimen. Shear stress here means the maximum value of the shear stress at the center of the side plane of the specimen. It was calculated by considering the anisotropy of wood, as shown in a previous report (Sasaki et al. 2004).

Failure surface

The failure surface was determined by the static tests described above, as a combination of axial and shear strength. A previous study (Sasaki and Yamasaki 2002) demonstrated that Hill's criterion could approximate the failure condition. In order to determine the combined-stress ratios for fatigue tests under combined loading, Hill's criterion was utilized. Based on the standardized Hill's criterion for each type of static strength, the combined-stress ratio for the fatigue tests was determined. Namely, the combined-stress ratio (β) was defined as the ratio of normalized axial stress to normalized shear stress. Five ratios (β), that is, combinations of axial and shear stresses (indicated as S, CA, CB, CC, and C), were used: β = 0:1 (pure torsion, indicated as S), −0.41:0.92 (CA), −0.73:0.71 (CB), −0.93:0.38 (CC), and −1:0 (pure compression, C). These β's equally divided the quadrant for compression-shear combined-stress states into four based on the failure criterion, as previously described (Sasaki et al. 2005). Each number indicated the ratio of the stress to pure compressive or shear strength (σ_A/F_A or τ_S/F_S). As determined from these ratios, the shear stress component is dominant in the combined-stress CA state, and the compressive stress component is dominant in the CC state. In the CB state, the shear and compressive stress components were almost equally applied. The values for each combination are shown in Table 2.

Fatigue tests

The testing machine used for the static tests, which could apply axial and torsional loads simultaneously, was also used for the fatigue tests. A pulsating triangular axial load of compression was applied in the longitudinal direction at 1 Hz while the specimen was also simultaneously subjected to a twisting moment. Stress level in the fatigue tests was determined as the ratio of the maximum stress to the ultimate stress on the basis of the values shown in Table 2. Four stages equivalent to 100, 90, 80, and 70% of these values were used as the stress levels. For each stress level, two to five specimens were tested. The total number of specimens used in the fatigue tests was 59. All tests were carried out at 25°C and a relative humidity of 40%.

Failures of the specimens in this study were recognized as follows: compression failure—when the compressive strain was greater than 1% or a failure line was clearly visible at the surface of the specimen, and torsion failure—when the chuck of the testing machine rotated up to $\pi/4$ rad. These standards for failure were based on the results of mechanical testing under static conditions.

TABLE 2. *Stress ratios and ultimate stresses in compression and shear.*

	Combined-stress ratio (β)		Ultimate stress [MPa]		
Combined-stress state	Axial	Shear	Axial (σ_{ult})	Shear (τ_{ult})	Remarks
S	0	1	0.00	23.5	Pure torsion
CA	0.41	0.92	−16.7	21.6	Combined compression
CB	0.74	0.71	−30.4	16.7	and shear
CC	0.93	0.38	−38.2	8.82	
C	1	0	−41.2	0.00	Pure compression

Each number of the combined-stress ratio (β) indicates the ratio of stress to pure compressive or pure shear strength, that is, σ_A/F_A or τ_S/F_S.

RESULTS AND DISCUSSION

Stress-strain relationship

Figure 1 shows examples of the stress-strain (*S-S*) diagrams obtained from the fatigue tests, in which the left panel shows the *S-S* diagrams for compression and the right panel shows the *S-S* diagrams for torsion. The combined-stress ratio shown in this figure was CB, and the stress level and number of cycles to failure (*Nf*) were 90% and 28,635 cycles, respectively. As shown in Table 2, the compressive and shear stress components in the CB state were almost equally applied.

Figure 1(a) depicted that the *S-S* diagrams hardly changed until the number of loading cycles (*n*) reached 22,909. The slope, residual compressive strain, and hysteresis loop area of the *S-S* diagram barely changed after $n = 1{,}000$. As previously described, residual tensile strain increased as the number of loading cycles (*n*) increased, but the slope of tensile *S-S* diagrams hardly changed under pulsating tension-torsion combined loading (Sasaki and Yamasaki 2004; Sasaki et al. 2005). The *S-S* diagrams under axial-torsion combined loading showed different performances of compression and tension. In contrast, the slope, residual shear strain, and hysteresis loop area of the *S-S* diagram changed as the number of loading cycles (*n*) increased, as shown in Fig. 1(b). Therefore, differences were observed in the slope and hysteresis loop area of the *S-S* diagrams. The change in the slope of the diagram indicates the behavior of the mechanical properties of wood during the fatigue process. In the following sections, the effects of pulsating combined loading on the change in this slope are examined.

During the combined loading tests, two *S-S* diagrams, one for axial and the other for shear, were obtained simultaneously as shown in Fig. 1. For each *S-S* diagram, the slope of a line that linked the two apexes of one loop, that is, the axial or shear secant modulus, was determined. The secant modulus is generally considered to correspond to the stiffness or apparent elastic modulus. In this study, the axial and shear secant moduli were interpreted as the axial and shear stiffness, respectively. Following a previous study, the compressive modulus and torsional rigidity were evaluated as the compressive and shear stiffness, respectively (Sasaki et al. 2004).

Compressive stiffness

Table 3 shows the compressive secant moduli at the first loading ($n = 1$) of each test. The average values ranged from 8.64 to 12.68 GPa. Examples of the relationships between compressive stiffness (= compressive secant modulus) and the number of loading cycles are described in Fig. 2. Compressive stiffness in the figure was normalized by the stiffness at the first loading ($n = 1$), as shown in Table 3.

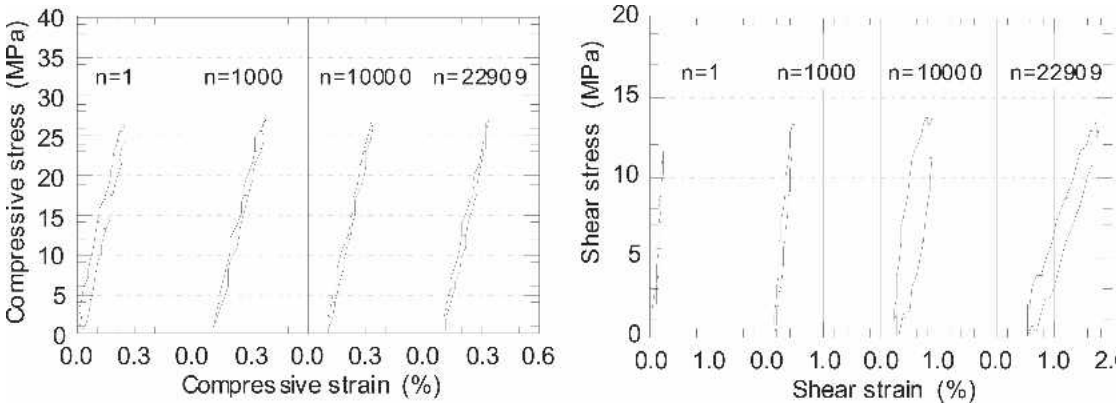

FIG. 1. Stress-strain relationships under pulsating compression-torsion combined loading (combined stress state: CB, stress level: 90%, *Nf* = 28635).

TABLE 3. *Compressive secant moduli (GPa) at the first loading.*

Combined-stress state	Stress level (%)			
	100	90	80	70
C	8.64 ± 0.28 (3)	9.54 ± 0.78* (2)	10.04 (1)	
CC	11.29 ± 2.26 (3)	11.79 ± 1.50* (2)	10.90 (1)	
CB	10.91 ± 0.53 (3)	11.16 ± 0.73 (3)	11.06 (1)	11.54 ± 0.82* (2)
CA	10.63 ± 1.11 (3)	10.08 ± 1.84* (2)	9.78 ± 0.12* (2)	12.68 ± 1.91* (2)

Numbers in columns indicate means ± standard deviations.
Numbers in parentheses indicate sample sizes.
* Numbers indicate means ± deviations.

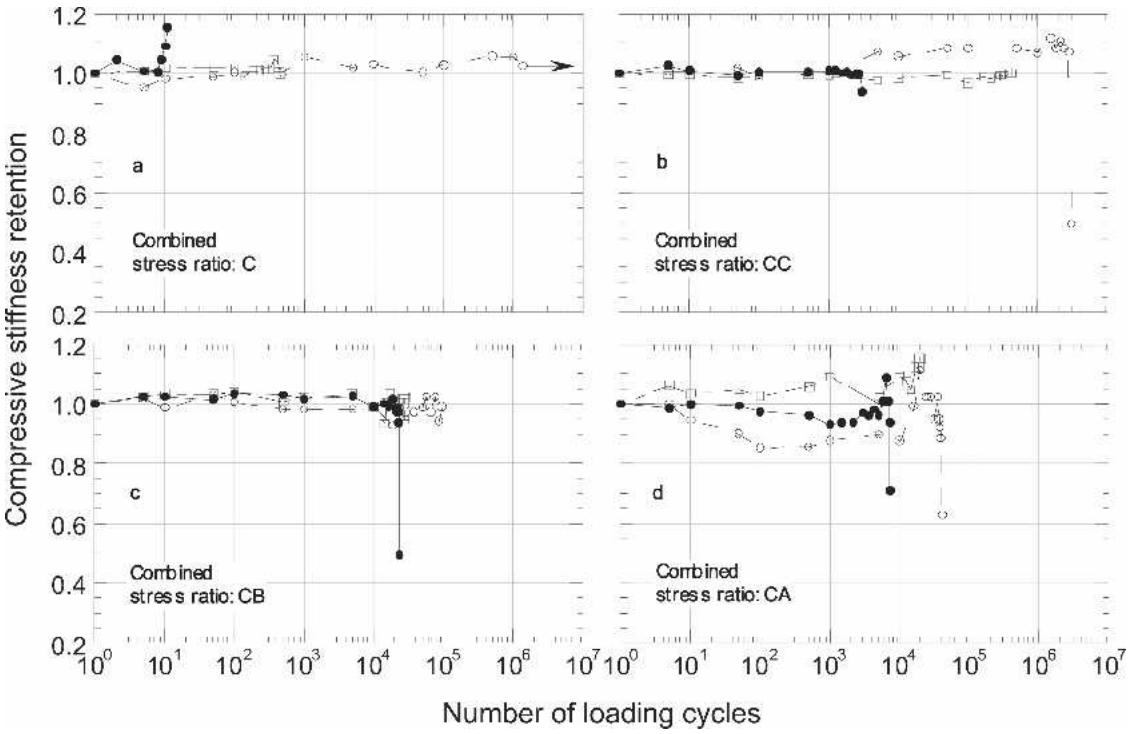

FIG. 2. Relationships between compressive stiffness retention and number of loading cycles at each combined-stress ratio. *Filled circles*, stress level 100%; *squares*, stress level 90%; *open circles*, stress level 80%.

Figure 2(a) shows compressive stiffness retention with the number of loading cycles in pure compressive fatigue tests (combined stress ratio: C). The compressive stiffness at each stress level maintained its initial value until final failure. That is, fatigue failure occurred without a decrease in compressive stiffness. Figure 2(b) explains the compressive stiffness retention in the combined compressive-torsion fatigue tests (CC). In the CC state, the compressive stress component was dominantly applied, and the shear stress component only slightly affected compressive stiffness retention. The overall tendencies in this state were slightly different from those seen in state C. Compressive stiffness maintained its initial value until final failure when the fatigue test was performed at higher stress levels (90 and 100%). However, when the test was performed at a stress level of 80%, compressive stiffness sharply decreased immediately before final failure.

In contrast, a previous study reported that the

tensile stiffness retention under tension-torsion combined loading showed differences between higher and lower stress levels (Sasaki and Yamasaki 2004). That is, tensile stiffness at higher stress levels (90 and 100%) maintained its initial value until final failure, and fatigue failure occurred without a decrease in tensile stiffness. When the test was performed at lower stress levels (60 and 70%), tensile stiffness began to decrease at about 0.1 of *Nf*, although it maintained its initial value until this decrease.

Figure 2(c) shows the compressive stiffness retention in the combined fatigue test under state CB where compressive and shear stress components were almost equally applied. The applied compressive stress in CB is smaller than those in C and CC. The trend in state CB was very similar to that observed in state CC. Compressive stiffness was maintained at an almost constant level from the beginning to the end of the fatigue test at lower stress levels (80 and 90%). On the other hand, compressive stiffness at a higher stress level (100%) was initially unchanged, and then suddenly decreased immediately before final failure. Figure 2(d) shows the compressive stiffness retention in the combined fatigue test under state CA, in which the shear stress component was dominantly applied. The applied compressive stress in state CA was smaller than in states C, CC, or CB. The overall tendencies in this state were notably different from those shown in Fig. 2(a)–(c). Compressive stiffness was unstable, and apparently increased at a late stage in the fatigue tests, and then suddenly decreased immediately before final failure. Such a tendency was remarkable in CA compared to CB and CC because the shear stress component in CA was larger than that in CB and CC. The failure mode under these test conditions was predominantly torsion failure, as described in the *Failure mode* section. Immediately before final failure, the specimen was markedly twisted, and the large rotational deformation was thought to affect the axial deformation. That is, the axial deformation was restrained by the large rotational deformation, and this resulted in an apparent increase in compressive stiffness.

Shear stiffness

Tables 4 and 5 show the shear secant moduli on the LR plane and the torsional rigidity at the first loading ($n = 1$). The average shear secant moduli ranged from 0.82 to 3.61 GPa, as shown in Table 4. The values in state CC are not listed in these tables because the applied shear stress in CC was the smallest in comparison with the others, and the readout of the stress-strain relationships was too unstable to evaluate the shear stiffness. One reason for this is that the loading capacity of the testing machine was too powerful to control small torsion against the wood specimen.

The values increased gradually in the CA and CB states, as the compressive stress component became dominant. The shear stiffness was reported to show an increase under conditions where application of compression was dominant (Yamasaki and Sasaki 2003). The relationship between shear stiffness and combined stress states showed clear trends under conditions where the axial force was applied dominantly. When a large compression was applied with torsion, warping of the specimen by torsion was

TABLE 4. *Shear secant moduli at the first loading.*

	Shear secant modulus (GPa)			
	Stress level (%)			
Combined-stress state	100	90	80	70
S	0.85 ± 0.15 (3)	0.94 ± 0.03* (2)	0.82 ± 0.14 (4)	0.88 ± 0.07 (4)
CA	2.10 ± 0.21 (3)	1.95 ± 0.53* (2)	2.20 ± 0.09* (2)	1.86 ± 0.46* (2)
CB	3.61 ± 1.82 (3)	3.55 ± 1.58 (3)	3.48 (1)	2.70 ± 1.39* (2)

Numbers in columns indicate means ± standard deviations.
Numbers in parentheses indicate sample sizes.
* Numbers indicate means ± deviations.

TABLE 5. *Torsional rigidity (10^3 GPa · mm^4) at the first loading.*

Combined-stress state	Stress level (%)			
	100	90	80	70
S	1.83 ± 0.33 (3)	1.93 ± 0.08* (2)	1.77 ± 0.30 (4)	1.89 ± 0.12 (4)
CA	4.08 ± 0.29 (3)	3.73 ± 0.73* (2)	4.86 ± 0.39* (2)	4.33 ± 0.14* (2)
CB	6.64 ± 0.16 (3)	7.69 ± 0.36 (3)	8.47 (1)	4.85 ± 0.23* (2)

Numbers in columns indicate means ± standard deviations.
Numbers in parentheses indicate sample sizes.
* Numbers indicate means ± deviations.

restrained. Under such conditions, the specimen is subjected to two types of torsional moment, a torsional moment caused by twisting of the specimen, and a secondary torsional moment caused by the restraint of warping. The cross-sectional force is the sum of these torsional moments (Wagner and Pretschner 1935; Komatsu 1969; Takaoka 1974). This may provide an explanation for the observation of increased shear stiffness, as the compressive stress component become dominant.

Figure 3 shows the relationship between shear stiffness (torsional rigidity) and the number of loading cycles. Shear stiffness was normalized based on the value at the first loading ($n = 1$), shown in Table 5. Figure 3(a) shows the shear stiffness retention in the pure torsion fatigue test (combined stress ratio: S). The shear stiffness in state S was initially almost constant with an increase in the number of loading cycles, and then decreased immediately before final failure, at all stress levels. When examined in detail, however,

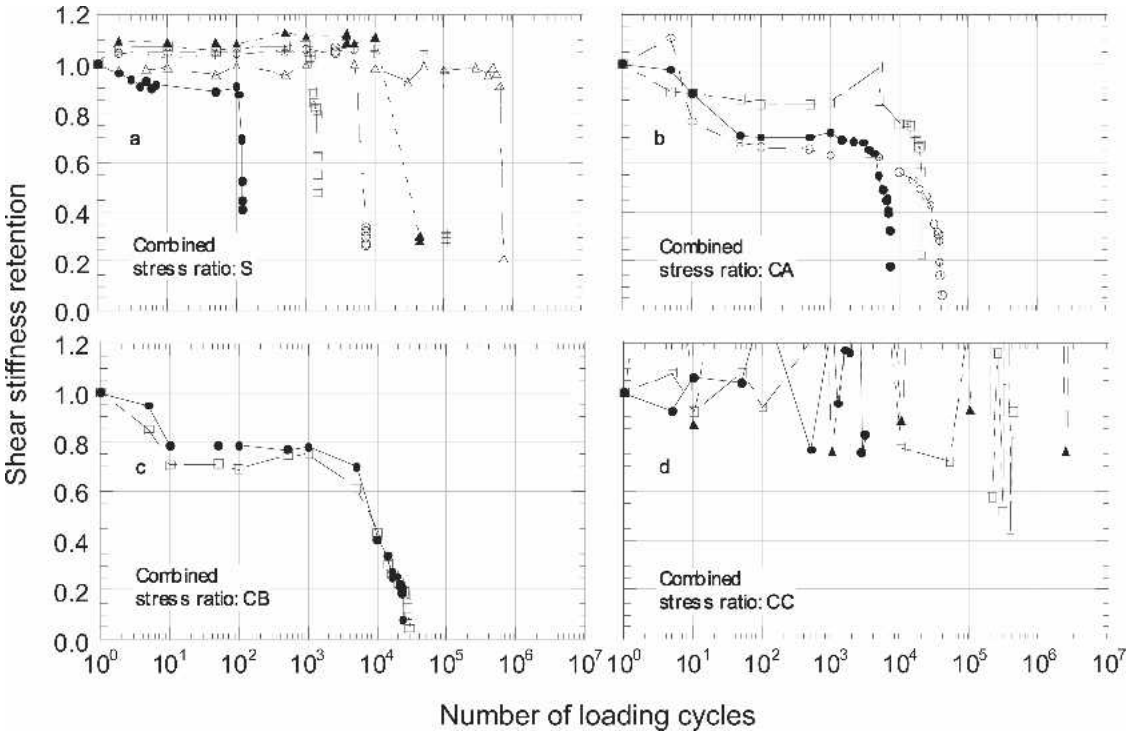

FIG. 3. Relationships between shear stiffness retention and the number of loading cycles at each combined-stress ratio. *Filled circles*, stress level 100%; *squares*, stress level 90%; *open circles*, stress level 80%; *filled triangles*, stress level 70%; *crosses*, stress level 60%; *open triangles*, stress level 50%.

the stiffness at higher stress levels (90%, 100%) began to decrease at about 0.7 of *Nf*, while the stiffness at lower stress levels (60%, 70%) decreased immediately before final failure. As the stress level in the fatigue test decreased, the final reduction of shear stiffness increased. Figure 3(b) shows the shear stiffness retention in CA, where the shear stress component was dominant in the combined-stress state. The overall tendencies of the shear stiffness retention seen in state CA were considerably different from those seen in state S. The stiffness retention decreased to 70%–80% immediately after loading at about 10^1–10^2 cycles; it then gradually decreased toward final failure. The final reduction of shear stiffness was larger than that in S (pure torsion) at all stress levels. In the stress states of S and CA, where the shear stress component was dominantly applied, shear stiffness showed a remarkable decrease toward final failure at all stress levels. This trend was different from that observed for compressive stiffness, and was attributed to the shear stress component. However, the process of shear stiffness retention showed significant differences between these combined stress states. Thus, the effects of compressive stress on shear stiffness were obvious under conditions of compression-shear combined stress. Figure 3(c) shows the shear stiffness retention in the combined fatigue test under state CB. The overall tendencies in this state were similar to those seen in state CA. The final reduction of shear stiffness in state CB was also larger than those observed in states CA and S. However, in state CB, fatigue life is almost the same at all stress levels, contrary to the case in states S and CA. Therefore, the influence of stress level on fatigue life is not clear in the CB state. This trend was also seen under the TB (tension-shear combined stress) state, as reported previously (Sasaki et al. 2004).

Figure 3(d) shows the shear stiffness retention in state CC, where the compressive stress component was dominantly applied. The applied shear stress in CC was the smallest among all stress ratios. Therefore, the trend of shear stiffness retention was not clear, although the compressive stiffness maintained its initial value during almost all fatigue processes, as seen in Fig. 2(b).

Although the shear stress amplitude was the same in both compression-torsion and tension-torsion combined loadings, as shown in a previous report (Sasaki et al. 2005), differences in shear stiffness retention were observed between these axial-torsion combined loadings. This suggests that the shear stiffness retention as the number of loading cycles increases is significantly influenced by β.

Failure mode

Figure 4 shows examples of the failure modes obtained in the fatigue tests performed under each combined-stress ratio. From left to right, these examples show pure torsion (S), combined-stress (CA, CB, CC), and pure compression (C) states, respectively, at a stress level of 100%. As shown in Fig. 4, in the S, CA, and CB states, where shear stress was applied dominantly, cracks along the fiber due to torsion failure were observed. On the other hand, failure lines were clearly visible at the surface of the specimens in the CC and C states, where compressive stress was applied dominantly. Therefore, the influence of the combined-stress ratio on the failure mode was determined. In addition, when the stress levels were reduced, almost the

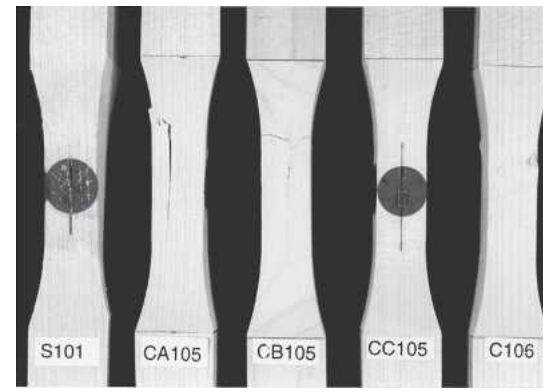

FIG. 4. Examples of failure modes observed during fatigue testing at a stress level of 100%. From left to right, typical failure modes under pure torsion (S), combined-stress (CA, CB, CC), and pure compression (C) states are shown.

same destructive tendencies as shown in Fig. 4 were observed.

The failure mode in the TB state, in which axial (tensile) and shear stresses were applied at equal levels, was affected by stress level, as shown in a previous report (Sasaki and Yamasaki 2004). The effect of tensile stress on failure became more significant at higher stress levels, while the effect of shear stress on failure became more significant at lower stress levels. In contrast, the failure mode in compressive-shear combined stress states was not affected by the stress level.

CONCLUSIONS

The trend toward lower stiffness retention differed between compression and shear stress, and was influenced by the combined-stress ratio (β). Compressive stiffness tended to maintain its initial value during almost all loading cycles to failure. Shear stiffness decreased with increased number of loading cycles, except in the stress state CC, where compression was dominant. The final decrease of shear stiffness was larger as compressive stress became dominant.

The failure mode was dramatically affected by the combined stress state; typical torsion failure was observed in the S, CA, and CB states, in which shear stress was dominantly applied. On the other hand, typical compression failure was observed in the CC and C states, in which compressive stress was applied dominantly. The failure mode under compressive-shear combined stress was not affected by the stress level; however, it was affected by the stress level under tensile-shear states.

REFERENCES

KOMATSU, S. 1969. Theory and calculation for thin-walled structures. I. Sankaido, Tokyo, Japan. 218 pp.

SASAKI, Y., AND M. YAMASAKI. 2002. Fatigue strength of wood under pulsating tension-torsion combined loading. Wood Fiber Sci. 34:508–515.

———, AND ———. 2004. Effect of pulsating tension-torsion combined loading on fatigue behavior in wood. Holzforschung 58:666–672.

———, ———, AND T. SUGIMOTO. 2005. Fatigue damage in wood under pulsating multiaxial-combined loading. Wood Fiber Sci. 37:232–241.

TAKAOKA, N. 1974. Torsion analysis of structural members. Kyoritsu Shuppan, Tokyo, Japan. Pp. 77–78.

WAGNER, H., AND W. PRETSCHNER. 1935. Verdrehung und Knickung von Offnen Profilen. Luftfahrtforshung 11:174–180.

YAMASAKI, M., AND Y. SASAKI. 2003. Elastic properties of wood with a rectangular cross section under combined static axial force and torque J. Mater. Sci. 38: 603–612.

———, AND ———. 2004. Yield behavior of wood under combined static axial force and torque. Exp. Mech. 44:221–227.